

Unlocking the potential of ultra-high dose fractionated radiation for effective treatment of glioblastoma

Xiao-Yan Lan

Dalian Municipal Central Hospital

Lukasz Kalkowski

University of Maryland Baltimore

Cheng-Yan Chu

University of Maryland Baltimore

Anna Jablonska

University of Maryland Baltimore

Shen Li

Capital Medical University

Mihoko Kai

Johns Hopkins University

Yue Gao

University of Maryland Baltimore

Mirosław Janowski

University of Maryland Baltimore

Piotr Walczak (✉ pwalczak@som.umaryland.edu)

University of Maryland Baltimore

Research Article

Keywords: glioblastoma, fractionated radiation, brain injury, vascular damage, hypoxia-inducible factor

Posted Date: November 1st, 2023

DOI: <https://doi.org/10.21203/rs.3.rs-3500563/v1>

License:  This work is licensed under a Creative Commons Attribution 4.0 International License.

[Read Full License](#)

Additional Declarations: Competing interest reported. Mirosław Janowski and Piotr Walczak are co-founders and co-owners of IntraART, LLC and Ti-Com, LLC., but they are not directly related to the content

of this study. Other co-authors declare no potential conflict of interest.

Abstract

Background: Conventional radiation therapy for glioblastoma (GBM) has limited efficacy. Regenerative medicine brings hope for repairing damaged tissue, opening opportunities for elevating the maximum acceptable radiation dose. In this study, we explored the effect of ultra-high dose fractionated radiation on brain injury and tumor responses in immunocompetent mice. We also evaluated the role of the HIF-1 α under radiation.

Methods: Naïve and hypoxia-inducible factor-1 alpha (HIF-1 α)^{+/-} heterozygous mice received a fractionated daily dose of 20 Gy for three or five consecutive days. Magnetic resonance imaging (MRI) and histology were performed to assess brain injury post-radiation. The 2 \times 10⁵ human GBM1 luciferase-expressing cells were transplanted with tolerance induction protocol. Fractionated radiotherapy was performed during the exponential phase of tumor growth. BLI, MRI, and immunohistochemistry staining were performed to evaluate tumor growth dynamics and radiotherapy responses. Additionally, animal lifespan was recorded.

Results: Fractionated radiation of 5 \times 20 Gy induced severe brain damage, starting 3 weeks after radiation. All animals from this group died within 12 weeks. In contrast, later onset and less severe brain injury were observed starting 12 weeks after radiation of 3 \times 20 Gy. It resulted in complete GBM eradication and survival of all treated animals. Furthermore, HIF-1 α ^{+/-} mice exhibited more obvious vascular damage 63 weeks after fractionated radiation of 3 \times 20 Gy.

Conclusion: Ultra-high dose fractionated 3 \times 20 Gy radiation can eradicate the GBM cells at the cost of only mild brain injury. The HIF-1 α gene is a promising target for ameliorating vascular impairment post-radiation, encouraging the implementation of neurorestorative strategies.

Background

Glioblastoma (GBM) is the most common primary central nervous system malignancy in adults;¹ the three-year survival rate of patients is only 10.3%.² This dismal clinical outcome highlights that treating GBM remains one of the greatest challenges in medicine.

Radiotherapy is an essential adjuvant strategy used in conjunction with other treatments.³ However, the negative impact of side effects, particularly on neurological and cognitive function,⁴ can significantly reduce the quality of life for patients after treatment. Furthermore, these side effects often set the threshold for the maximum tolerable levels of anti-tumor radiation therapies that can be administered. Several targeted therapeutic techniques have been developed to address these issues, including three-dimensional conformal radiation therapy,⁵ intensity-modulated radiation therapy,⁶ hyper-fractionated radiotherapy,⁷ and functional imaging-guided dose-escalated radiation therapy.⁸ These techniques can selectively destroy the bulk of the tumor. Unfortunately, the early invasive growth of GBM, with satellite

cancer cells found within the brain far from the tumor mass, makes conformal radiation therapy prone to a high recurrence rate. As a result, there is a dire need for a breakthrough treatment.

The field of regenerative medicine has advanced tremendously in recent years, paralleling the progress in oncology. However, these fields have not yet been sufficiently integrated, leaving many untapped opportunities. Regenerative medicine techniques now enable the repair and replacement of damaged white matter and vasculature, the tissue components most vulnerable to radiation damage.⁹ It presents an exciting opportunity for elevating the maximum acceptable dose of radiation. Combining ultra-high dose fractionated radiation therapy with brain repair techniques may be feasible to achieve effective brain tumor eradication. In addition, we sought to explore the mechanism of radiation-induced vascular damage. To do so, we studied hypoxia-inducible factor-1 alpha (HIF-1 α) signaling, a well-established system that is a master regulator of endothelial homeostasis and angiogenesis.¹⁰ HIF-1 α signaling has not been systematically studied in the context of responses to radiation injury, and the modulation of HIF-1 α signaling has not been exploited as a therapeutic strategy for brain radiation injury. In this study, we explored the efficiency of ultra-high dose fractionated radiation therapy for human GBM in immunocompetent mice using the described immunological tolerance induction protocol.¹¹ We also investigated radiation-induced brain injury in both wild-type mice and HIF-1 α ^{+/-} heterozygote mice to better understand the role of HIF-1 α signaling in radiation-induced vascular damage.

Methods

Animal irradiation

All procedures involving live animals were approved and performed in accordance with the Guide for the Care and Use of Laboratory Animals at the local Animal Care and Use Committee. Ten naïve C57BL/6J mice (8–10 weeks (w), 20–25 g, Jackson Laboratory), as well as 12 transgenic HIF-1 α ^{+/-} mice (which are heterozygous for a null (knockout) allele at the locus encoding HIF-1 α) and 12 wild-type mice of the same litter (6–8 w, both provided by Prof. Gregg L. Semenza), received fractionated daily dose of 20 Gy radiation for consecutive three (Fr 3 \times 20 Gy) or five (Fr 5 \times 20 Gy) days. Briefly, the mice were anesthetized with isoflurane (4% for induction, 1%-2% for maintenance) and placed in the prone position. A custom-built small animal radiation research platform (SARRP) equipped with onboard computed tomography (CT)-guidance was used for radiotherapy. Following three-dimensional CT acquisition, a target spot (2.5 mm deep relative to the skull) was irradiated with a single beam (60° angle), using a 5 \times 5 mm² collimator at a daily dose of 20 Gy for three consecutive or five days.

Magnetic resonance imaging

Magnetic resonance imaging (MRI) was performed under general anesthesia (isoflurane) after radiation 1 w, 3 ws, 5 ws, and then monthly until the mice deteriorated or reached the end of our observation time. Mice were placed on a water-heated animal bed equipped with temperature and respiratory control. All MRI experiments were performed on a horizontal bore 11.7 T Bruker Biospec system (Bruker, Ettlingen,

Germany), and a surface coil array was used for image acquisition. Baseline T2 (repetition time (TR)/echo time (TE) = 2500/30 ms, slice thickness (ST) = 0.7 mm, average (AV) = 2, the field of view (FOV) = 14 × 14 mm², matrix size = 256 × 256, RARE factor = 8) and T1 (TR/TE 350/6.7 ms, AV = 2)-weighted images of the brain were acquired. Gadolinium (30 µL) was injected intraperitoneally (i.p.) for contrast-enhanced T1 scans, and T1 post-gadolinium images were acquired.

Cell Culture

The human GBM1 luciferase-expressing cells were kindly provided by Dr. Charles Eberhart from Johns Hopkins University. Cells were expanded in culture medium (Neurobasal-A Medium and DMEM/F12 (1:1), Thermo Fisher Scientific) containing B27 without vitamin A (Thermo Fisher Scientific), 20 ng/mL human EGF (Peprotech), 20 ng/mL human bFGF (Peprotech) and 2 µg/mL heparin (Sigma). All cells were suspension cultured as neurospheres in a humidified atmosphere of 5% CO₂ at 37°C.

Tumor implantation

Fifteen male C57BL/6J mice (6–8 w, 20–25 g, Jackson Laboratory) were used for tumor transplantation. Animals were randomly assigned to three groups: GBM1 without radiation (GBM1, n = 5), GBM1 with a fractionated daily dose of 2 Gy (GBM1 + Fr 3×2 Gy, n = 5) or 20 Gy (GBM1 + Fr 3×20 Gy, n = 5) for consecutive three days. Before transplantation, GBM1 oncospheres were harvested, dissociated into single cells, and suspended in PBS at a final concentration of 1×10⁵/µL. Then animals were anesthetized with isoflurane. A total number of 2×10⁵ cells were injected at a rate of 1 µL/min into the right striatum (anteroposterior = 0.5 mm; mediolateral = 2.0 mm; dorsoventral = 2.5 mm) using a 10 µL Hamilton syringe with an attached 31-gauge needle. After injection, the needle was kept in place for 2 minutes (min) to avoid backflow of the injected cells through the needle tract and then withdrawn.

To induce immunological tolerance to xenografted human tumors in immunocompetent C57BL/6J mice, hamster anti-mouse CD154mAb (MR1, BioXcell, Lebanon, NH) and CTLA-4-Ig (Abatacept, Bristol-Myers Squibb, Princeton, NJ) were administered to animals (500 µg each) i.p. on days 0, 2, 4, and 6 after tumor inoculation. The weight changes and neurological symptoms of mice were recorded twice a week. Bioluminescence imaging (BLI) was used to monitor tumor growth rate and was initiated a day after tumor implantation. Fractionated radiotherapy (Fr 3×2 Gy or Fr 3×20 Gy) was performed after tumor inoculation when BLI showed accelerating tumor growth. Then BLI and MRI were performed to assess the tumor response and brain injury.

Bioluminescence imaging

Animals were anesthetized with isoflurane and injected i.p. with 150 µl luciferin (30 mg/mL, Gold Biotechnology). Images were acquired 5–15 min after substrate injection at the peak of the bioluminescence signal by IVIS Spectrum In Vivo Imaging System (PerkinElmer). For BLI analysis, images were quantified by drawing regions of interest (ROIs). The data were expressed as photon flux (p/sec). Imaging began on day 1 post-implantation and was then done weekly within the first month, biweekly

within the second month, and monthly after that until the mice deteriorated or reached the end of our observation time.

Behavior Assessment

Open-field test: Open-field test was performed using the SDI Open Field System (San Diego Instruments, San Diego, CA). The open field arena was a 20×40 cm Lexan shoebox cage equipped with a camera to monitor overall locomotor activity. For each open-field test session, mice were placed in the center of the field, and activity was monitored for 5 min. In addition, the travel distance and average speed were measured by the investigator blind to the study design.

Y-maze test: Mice were placed at the end of one of the three arms and allowed to explore freely for 5 min. Spatial recognition memory was assessed. The testing was video recorded, and the number of times the mouse entered three different arms consecutively divided by the total visits were measured by an observer blind to the condition.

Histological analysis

Mice were deeply anesthetized with isoflurane and perfused intracardially with 5% sucrose, followed by 4% paraformaldehyde (PFA). Brains were dissected, post-fixed in 4% PFA overnight at 4 °C, then successively cryopreserved in 20% and 30% sucrose until the tissue sank. Brains were cryosectioned into 30- μ m-thick coronal sections. Hematoxylin and eosin (H&E) staining was performed. For eriochrome cyanin staining, slides were oven-dried and dehydrated in 95% and 70% ethanol, then put into the eriochrome cyanine solution (0.2% eriochrome cyanine, 0.4% FeCl₃, and 0.5% H₂SO₄). Staining was developed by alternating exposure to 0.1% NH₄OH for 3–7 s and rinsing in distilled water for 30 s until the blue background was reduced, and the cells turned faintly pink but still had blue shading. After that, sections were put in two changes of 70%, 95%, and 100% ethanol and three changes of xylene for 10 min each.

For immunofluorescence staining, the sections were blocked using 0.1% Triton and 2% BSA for 1 h at room temperature and then incubated overnight with primary antibodies at 4°C. In addition, either Alexa-488 or Alexa-555 (Molecular Probes, 1:200) secondary antibody was added for 2 h incubation at room temperature. Sections were then counterstained with mounting medium with DAPI (VectaStain, Vector Labs). The following primary antibodies were used: human-nuclear antigen (HuNu, 1:250; Cat. MAB1281, Millipore), GFAP (1:250; Cat. Z0334, Dako), NeuN (1:100; Cat. D3S3I, Cell Signaling Technology), Iba1 (1:250; Cat. 019-19741, Wako); CD45 (1:250; Cat. ab10558, Abcam), Collagen IV (1:300; Cat. ab6586, Abcam). Histochemical and immunofluorescent images were acquired with a DMi8 inverted microscope (Leica Microsystems). For quantification, images of entire brain tissue (three to five brain tissue sections per mouse) were captured with 5× magnification. In addition, the intensities of the ipsilateral or contralateral hemisphere were measured by Image J (Version 1.52p, USA).

Statistical analysis

The overall mouse survival time was calculated and expressed by the Kaplan-Meier curve, and the statistical difference was analyzed by log-rank tests. The Shapiro-Wilk test was used to test if the distribution was normal. Those results were presented as mean \pm standard deviation (SD). The intergroup differences between more than 2 groups were assessed using ANOVA followed by a post-hoc the least significance difference (LSD) test. The comparison of 2 groups was evaluated using an independent t-test. Data without normal distribution were presented as median with interquartile range (IQR). The Mann-Whitney test was used when comparing two groups, and the Kruskal-Wallis test was used when comparing more than 2 groups. All statistical analysis was performed using the SPSS software package (Version 22.0, USA). $P < 0.05$ was considered to be statistically significant.

Results

Ultra-high dose fractionated radiation leads to late-phase brain injury

We studied the effects of ultra-high dose radiation on the brain of immunocompetent mice. The mice were exposed to two radiation doses, 60 Gy divided into 3 fractions and 100 Gy divided into 5 fractions delivered daily. Longitudinal MRI showed that Fr 5 \times 20 Gy radiation-induced multiple microhemorrhages starting from 3 weeks after radiation (Fig. 1A-B) and that was accompanied by blood-brain barrier (BBB) breakdown (Fig. 1C-D). Additionally, we observed white matter damage and brain edema as evidenced by the ipsilateral lateral ventricle compression 8 weeks after Fr 5 \times 20 Gy radiation (Fig. 1E-G). Most of the Fr 5 \times 20 Gy animals showed sudden deterioration, and all mice died within 12 weeks (Fig. 1H).

Fractionated radiation of 3 \times 20 Gy also caused brain damage, but the damage was observed much later, after three months. Animals developed vascular abnormalities manifested as microbleeds and BBB breakdown, first observed 12 weeks after radiation (Fig. 1A-D). At 79 weeks after radiation, we observed compression of the lateral ventricle on the ipsilateral side (Fig. 1E-G). We conducted histological staining in the very late stage (80 weeks) after radiation to further assess brain damage. As shown in Fig. 2, only mild demyelination (Eriochrome, MBP) and vascular abnormalities (Collagen IV) were observed. Minor neuroinflammation, including astrocyte (GFAP) or microglia (Iba1)/macrophage (CD68) activation, was detected at 80 weeks. However, we found no neuronal loss (NeuN) even at that late time. All mice from the Fr 3 \times 20 Gy group survived as long as 80 weeks (the end of our observation time) post-irradiation. Therefore, this dose was selected for further GBM1 eradication studies. The remarkably long window encourages further study to identify targets and opportunities to implement therapeutic intervention addressing the observed damage.

Fractionated 3 \times 20 Gy radiotherapy eradicated GBM in immunocompetent mice

The GBM1 tumor xenograft tolerance model was successfully established in the brain of immunocompetent recipients, and its growth was monitored with BLI and MRI. Tumors grew rapidly, as shown by both imaging modalities (Fig. 3). Radiotherapy (Fr 3×2 Gy (a lower dose used as clinically-relevant therapy control) or Fr 3×20 Gy) was performed when BLI showed exponential tumor growth and T2 MRI showed a visible tumor mass around 25 days after tumor inoculation. All the untreated tumor-bearing mice died within 9 weeks. A lower dose of Fractionated 3×2 Gy irradiation slowed the tumor growth and slightly prolonged animal survival; however, all mice died within 14 weeks. In animals treated with ultra-high dose fractionated 3×20 Gy radiation, the bioluminescence signal of the tumor gradually disappeared and overlapped with background radiance (Fig. 3A-B). MR images one month later showed regression of cancer with some hypointensity at the tumor site (Fig. 3C). No tumor regrowth was observed even at 46 weeks after radiation, as evidenced by MRI (Fig. 3C). Negative HuNu (a marker of human cell nucleus) and Stem121 (a marker of human cell cytoplasm) staining also confirmed the disappearance of the GBM1 tumor (Fig. 3E-F), and there was a dramatic improvement in survival for up to 322 days (the end of our observation time, Fig. 3D).

HIF-1 α deficiency exacerbates local vascular damage after radiation

We further evaluated the role of the HIF-1 α gene in radiation-induced brain injury. Fractionated 5×20 Gy radiation-induced severe brain injuries in HIF-1 α ^{+/-} heterozygote and wild-type mice. In T2*, hypointensity appeared starting at week 3 after irradiation (Supplementary Fig. 1A-B), indicating microhemorrhages. In addition, there was widespread BBB breakdown starting 3 weeks after radiation, as evidenced by Gd enhancement on T1 images (Supplementary Fig. 1C-D). The ipsilateral/contralateral hemisphere and lateral ventricle areas were measured on T2 images, which showed a volume increase at 8 weeks, probably due to hemorrhage and edema, and then reduced at 12 weeks, indicating brain atrophy (Supplementary Fig. 1E-F). However, we did not observe a significant difference in the severity of the above brain damage measures between HIF-1 α ^{+/-} and wild-type mice under this dose treatment.

There was no apparent brain injury before 16 weeks post-fractionated 3×20 Gy irradiation. However, animals developed vascular abnormalities manifested as microbleeds and BBB breakdown at 63 weeks after radiation in both HIF-1 α ^{+/-} heterozygote and wild-type mice (Fig. 4A-D). In addition, at 63 weeks, we observed compression on the ipsilateral side, indicating microhemorrhages and/or brain edema (Fig. 4E-F). Neither neurobehavioral manifestation (open-field and Y-maze tests) nor survival time showed the difference between HIF-1 α ^{+/-} heterozygote mice and wild-type mice under any radiation dose (Supplementary Fig. 2). Yet it is worth noting that, compared with wild-type mice, there was a clear trend towards more microhemorrhages, more extensive BBB breakdown, and more ipsilateral lateral ventricle compression in HIF-1 α ^{+/-} heterozygote mice (Fig. 4).

Furthermore, the HIF-1 α ^{+/-} mice exhibited higher levels of IgG leakage, which is considered one of the markers of vascular disruption (Fig. 5). Additionally, we observed malformation of blood vessels, as

characterized by increased vessel diameter in the brain tissue of HIF-1 α ^{+/-} mice (Fig. 5). These results indicate that HIF-1 α gene deficiency exacerbates vascular damage after radiation.

Discussion

Glioblastoma is characterized by infiltrative growth, intracerebral metastases, and resistance to chemotherapy, completely eradicating after standard treatment regimens (surgical resection followed by radiotherapy plus concomitant and adjuvant temozolomide) extremely difficult.¹²⁻¹⁴ Unfortunately, patients often face a high rate of recurrence and dismal prognosis. While increasing the radiotherapy dose may improve the success rate, it inevitably leads to brain damage. Actively dividing cells, including oligodendrocytes, vascular endothelium, and various precursor cells, are particularly vulnerable to this damage. Therefore, severe side effects preclude higher doses of radiotherapy.¹⁵ This gloomy reality has dominated for decades, but there is hope for a long-awaited breakthrough, thanks to new developments in regenerative medicine. While cell replacement strategies for brain repair have brought mixed results and have yet to prove successful in replacing neurons, replacing glial cells^{16,17} or vascular components¹⁸ is highly feasible. It creates an opportunity for innovation in treating GBM by escalating the radiotherapy dose followed by restorative therapy.

Our initial studies have shown that elevating the single dose of radiotherapy to as high as 80 Gy in mice is well tolerated over several weeks (data not shown), which is encouraging as this time window would allow regenerative intervention. However, despite an initial tumor response, the tumor could not be entirely eradicated, and recurrence was observed within two weeks. Therefore, we explored the effect of ultra-high dose fractionated radiation for brain tumor eradication and found that a fractionated 3 \times 20 Gy radiation dose can fully eradicate the tumor and significantly extend the survival time of mice while only resulting in mild brain injury over 12 weeks.

A variety of glial cells are extremely vulnerable to irradiation. These include astrocytes and microglia,¹⁹ but, most importantly, the oligodendrocytes and oligodendrocyte progenitor cells.²⁰ Oligodendrocytes are post-mitotic cells that provide a myelin sheath for neurons, and it has been shown that oligodendrocytes undergo continuous turnover and are replaced by local tissue progenitors.^{21,22} Depletion of these cells has been reported to occur as early as 3 days after irradiation,²³ ultimately resulting in demyelination and white matter loss, which are features typically associated with post-irradiation brain atrophy. Astrocytes are another important glial phenotype to consider. Given their recently elevated functionality, including maintaining potassium and neurotransmitter homeostasis, calcium signaling, and the production of cytokines, as well as playing a critical role in the formation of the BBB,²⁴ it is warranted to assess the contribution of astrocytes to radiation injury, and consider them as a therapeutic target.

The vascular consequences of radiotherapy have been relatively well characterized and include early and chronic effects in the brain.^{25,26} Early effects manifest as denuding endothelial cells, parenchymal cell damage, and exhaustion of the cell renewal system. It is followed by abnormal proliferation of the

endothelial cells, which are critical components of vascular remodeling, occurring months after the initial exposure. It has been shown that clinically relevant doses of ionizing radiation cause changes in the permeability of the BBB due to the abnormal synthesis of multiple proteins.²⁷ Vascular changes tend to predominate and can range from thrombosis, hemorrhage, and hyalinization to fibrinoid necrosis, which can further exacerbate the hypoxic/ischemic necrosis in the area. Critical to the feasibility of our study is the slow development of vascular abnormalities, which, while preceding necrosis, still require a long time to evolve.²⁶

Inadequate repair of damaged endothelial cells and BBB disruption after radiation exposure increase hypoxia in the local microenvironment, leading to upregulation of hypoxia-inducible factors HIF-1 α and HIF-2 α are master transcription factors for the cellular response to hypoxia.²⁸ Inhibition of HIF-1 activity is believed to have therapeutic benefits in tumor treatment.²⁹ Oligodendrocyte precursor cells (OPCs) are particularly susceptible to oxidative stress and radicals due to their low levels of anti-oxidants and free radical scavengers.^{30,31} It has been shown that oligodendrocytes and OPCs, play a central role in cerebral angiogenesis *via* HIF signaling. Yuen et al. found that constitutive HIF-1/2 α stabilization led to OPC maturation arrest, induced excessive postnatal angiogenesis *in vivo*, and directly stimulated (in a paracrine mechanism) endothelial cell proliferation *in vitro*.

Conversely, OPC-specific HIF-1/2 α loss of function led to insufficient angiogenesis in the corpus callosum and extensive axonal loss.³² These findings point to critical interactions between OPCs, angiogenesis, and axonal integrity, with HIF signaling being a master regulator. Dysregulation of this system during radiation therapy may be the focal point in the pathomechanism of radiation-induced brain injury. Indeed, this is highly feasible, as the early elimination of OPCs after radiotherapy removes their pro-angiogenic role and leads to the deterioration of endothelial cells. The exact mechanism could also contribute to the failed recruitment of new pro-angiogenic precursors despite their presence in circulating blood. Our study evaluated the status of HIF signaling after ultra-high dose radiotherapy and showed that HIF-1 α deficiency aggravated local vascular damage after radiation. This important result provides initial evidence for developing a strategy to prevent radiation injury *via* intervening with HIF-1 α signaling.

Regenerative strategies offer the potential to alleviate or even eliminate the side effects of anti-tumor treatment.¹⁷ An important implication is an opportunity to elevate radiation doses beyond the currently acceptable maximum dose. There is a precedent for this approach in hematology, where treating malignancies involves delivering a high dose of chemo/radiotherapy to the whole body, thereby completely destroying the tumor cells and hematopoietic stem cells; however, these stem cells can be restored via bone marrow transplantation.³³ This method is now a standard of care, with spectacular outcomes and, frequently, a complete cure for some malignancies.³⁴ Similarly, repairing or replacing damaged glial and vascular components after radiation injury seems feasible. Highly potent neural progenitor populations, such as glial-restricted progenitors and human neural progenitor cells transduced with GDNF, have been shown to replace endogenous dysfunctional glia in myelin disease models or amyotrophic lateral sclerosis.^{35,36} Moreover, the feasibility of an oligodendrocyte replacement strategy

after low-dose radiotherapy has been demonstrated but without tumor eradication.¹⁷ In our study, we take this approach a step further by using a higher radiation dose (60 Gy delivered as three daily fractions of 20 Gy each) to completely eliminate the tumor and investigate the possibility of preventing late-stage white matter and vascular damage through a regenerative strategy.

An additional strength of our study is the use of immunocompetent mice, which better mimic the tumor-host interactions observed in patients. Most human tumors are established in immunodeficient recipient mice (*nude/rag2/scid*) to prevent xenograft rejection, but this approach lacks an adaptive immune system, limiting its relevance for studying anti-tumor treatment. In contrast, our use of C57Bl/6J immunocompetent mice under a tolerance induction regimen allowed us to investigate the effects of aggressive radiotherapy in a more clinically relevant brain tumor model. To accomplish this, we have developed a successful strategy to induce tolerance for human brain tumor xenografts using antibodies blocking co-stimulatory signaling on T-cells.¹¹ This approach not only allowed us to gain insights into the biological characteristics and molecular mechanisms of GBM but also provided a suitable platform for investigating more effective therapeutic strategies, such as allogeneic stem cell transplantation, for this devastating disease.

Overall, we propose a completely new approach for treating brain tumors with the perspective of using regenerative medicine methods. We have demonstrated that supportive cellular components in the brain (glia and vasculature) are radio-sensitive but also have the potential to be replaced, which could open entirely new treatment paradigms for neoplastic conditions in the brain. This approach could be applied to chemotherapy, where targeted intraarterial delivery techniques are now available but cannot be fully exploited due to excessive toxicity. Finally, our findings shed light on the consequences and therapeutic targets of extremely high doses of radiation, which could be relevant in the context of nuclear accidents or catastrophes. Furthermore, we utilized immunocompetent mice, which provide a more clinically relevant model for investigating brain tumor-host interactions and testing therapeutic strategies. Overall, our study offers new insights into the use of regenerative medicine in treating brain tumors and provides a foundation for future research in this area.

Declarations

Ethics approval and consent to participate

All procedures involving live animals were approved and performed in accordance with the Guide for the Care and Use of Laboratory Animals at the local Animal Care and Use Committee.

Consent for publication

Not applicable

Availability of data and materials

Data presented in this study are available on request from the corresponding author. Moreover, all the deidentified data related to the study is available from the corresponding author on reasonable request.

Competing interests

Mirosław Janowski and Piotr Walczak are co-founders and co-owners of IntraART, LLC and Ti-Com, LLC., but they are not directly related to the content of this study. Other co-authors declare no potential conflict of interest.

Funding

This study was supported by NIH/NINDS under Grant NS102675-01A1.

Authors' contributions

Xiao-Yan Lan: Conceptualization, Methodology, Investigation, Data Curation, Writing- Original Draft

Lukasz Kalkowski: Conceptualization, Methodology, Investigation, Writing - Original Draft

Cheng-Yan Chu: Investigation

Anna Jablonska: Investigation, Formal analysis, Writing - Review & Editing

Shen Li: Investigation

Mihoko Kai: Conceptualization, Resources

Yue Gao: Investigation

Mirosław Janowski: Conceptualization, Methodology, Formal analysis, Writing - Review & Editing

Piotr Walczak: Conceptualization, Methodology, Supervision, Project administration, Funding acquisition

Acknowledgements

Not applicable

References

1. Ostrom QT, Price M, Neff C, et al. CBTRUS Statistical Report: Primary Brain and Other Central Nervous System Tumors Diagnosed in the United States in 2015-2019. *Neuro Oncol.* 2022;24(Suppl 5):v1-v95. doi:10.1093/neuonc/noac202
2. deSouza RM, Shaweis H, Han C, et al. Has the survival of patients with glioblastoma changed over the years? *Br J Cancer.* 2016;114(2):146-150. doi:10.1038/bjc.2015.421
3. Sulman EP, Ismaila N, Armstrong TS, et al. Radiation Therapy for Glioblastoma: American Society of Clinical Oncology Clinical Practice Guideline Endorsement of the American Society for Radiation

- Oncology Guideline. *J Clin Oncol*. 2017;35(3):361-369. doi:10.1200/jco.2016.70.7562
4. Laack NN, Brown PD. Cognitive sequelae of brain radiation in adults. *Semin Oncol*. 2004;31(5):702-713. doi:10.1053/j.seminoncol.2004.07.013
 5. Chan JL, Lee SW, Fraass BA, et al. Survival and failure patterns of high-grade gliomas after three-dimensional conformal radiotherapy. *J Clin Oncol*. 2002;20(6):1635-1642. doi:10.1200/jco.2002.20.6.1635
 6. Tsien CI, Brown D, Normolle D, et al. Concurrent temozolomide and dose-escalated intensity-modulated radiation therapy in newly diagnosed glioblastoma. *Clin Cancer Res*. 2012;18(1):273-279. doi:10.1158/1078-0432.Ccr-11-2073
 7. Miwa K, Matsuo M, Ogawa S, et al. Hypofractionated high-dose irradiation with positron emission tomography data for the treatment of glioblastoma multiforme. *Biomed Res Int*. 2014;2014:407026. doi:10.1155/2014/407026
 8. Laack NN, Pafundi D, Anderson SK, et al. Initial Results of a Phase 2 Trial of (18)F-DOPA PET-Guided Dose-Escalated Radiation Therapy for Glioblastoma. *Int J Radiat Oncol Biol Phys*. 2021;110(5):1383-1395. doi:10.1016/j.ijrobp.2021.03.032
 9. Yang L, Yang J, Li G, et al. Pathophysiological Responses in Rat and Mouse Models of Radiation-Induced Brain Injury. *Mol Neurobiol*. 2017;54(2):1022-1032. doi:10.1007/s12035-015-9628-x
 10. Rey S, Semenza GL. Hypoxia-inducible factor-1-dependent mechanisms of vascularization and vascular remodelling. *Cardiovasc Res*. 2010;86(2):236-242. doi:10.1093/cvr/cvq045
 11. Lan X, Kedziorek DA, Chu C, et al. Modeling human pediatric and adult gliomas in immunocompetent mice through costimulatory blockade. *Oncoimmunology*. 2020;9(1):1776577. doi:10.1080/2162402x.2020.1776577
 12. Stavrovskaya AA, Shushanov SS, Rybalkina EY. Problems of Glioblastoma Multiforme Drug Resistance. *Biochemistry (Mosc)*. 2016;81(2):91-100. doi:10.1134/s0006297916020036
 13. Han SJ, Englot DJ, Birk H, et al. Impact of Timing of Concurrent Chemoradiation for Newly Diagnosed Glioblastoma: A Critical Review of Current Evidence. *Neurosurgery*. 2015;62 Suppl 1(Suppl 1):160-165. doi:10.1227/neu.0000000000000801
 14. Lee SY. Temozolomide resistance in glioblastoma multiforme. *Genes Dis*. 2016;3(3):198-210. doi:10.1016/j.gendis.2016.04.007
 15. Balentova S, Adamkov M. Molecular, Cellular and Functional Effects of Radiation-Induced Brain Injury: A Review. *Int J Mol Sci*. 2015;16(11):27796-27815. doi:10.3390/ijms161126068
 16. Li S, Oh BC, Chu C, et al. Induction of immunological tolerance to myelinogenic glial-restricted progenitor allografts. *Brain*. 2019;142(11):3456-3472. doi:10.1093/brain/awz275
 17. Piao J, Major T, Auyeung G, et al. Human embryonic stem cell-derived oligodendrocyte progenitors remyelinate the brain and rescue behavioral deficits following radiation. *Cell Stem Cell*. 2015;16(2):198-210. doi:10.1016/j.stem.2015.01.004

18. Zampetaki A, Kirton JP, Xu Q. Vascular repair by endothelial progenitor cells. *Cardiovasc Res*. 2008;78(3):413-421. doi:10.1093/cvr/cvn081
19. Liu Q, Huang Y, Duan M, Yang Q, Ren B, Tang F. Microglia as Therapeutic Target for Radiation-Induced Brain Injury. *Int J Mol Sci*. 2022;23(15):8286. doi:10.3390/ijms23158286
20. Lee RX, Tang FR. Radiation-induced neuropathological changes in the oligodendrocyte lineage with relevant clinical manifestations and therapeutic strategies. *Int J Radiat Biol*. 2022;98(10):1519-1531. doi:10.1080/09553002.2022.2055804
21. Sock E, Wegner M. Transcriptional control of myelination and remyelination. *Glia*. 2019;67(11):2153-2165. doi:10.1002/glia.23636
22. Wang JQ, Gao MY, Gao R, Zhao KH, Zhang Y, Li X. Oligodendrocyte lineage cells: advances in development, disease, and heterogeneity. *J Neurochem*. 2022;164(4):468-480. doi:10.1111/jnc.15728
23. Chari DM, Gilson JM, Franklin RJM, Blakemore WF. Oligodendrocyte progenitor cell (OPC) transplantation is unlikely to offer a means of preventing X-irradiation induced damage in the CNS. *Experimental Neurology*. 2006;198(1):145-153. doi: 10.1016/j.expneurol.2005.11.023
24. Endo F, Kasai A, Soto JS, et al. Molecular basis of astrocyte diversity and morphology across the CNS in health and disease. *Science*. 2022;378(6619):eadc9020. doi:10.1126/science.adc9020
25. Park HJ, Griffin RJ, Hui S, Levitt SH, Song CW. Radiation-induced vascular damage in tumors: implications of vascular damage in ablative hypofractionated radiotherapy (SBRT and SRS). *Radiat Res*. 2012;177(3):311-327. doi:10.1667/rr2773.1
26. Greene-Schloesser D, Robbins ME, Peiffer AM, Shaw EG, Wheeler KT, Chan MD. Radiation-induced brain injury: A review. *Front Oncol*. 2012;2:73. doi:10.3389/fonc.2012.00073
27. Lee WH, Warrington JP, Sonntag WE, Lee YW. Irradiation alters MMP-2/TIMP-2 system and collagen type IV degradation in brain. *Int J Radiat Oncol Biol Phys*. 2012;82(5):1559-1566. doi:10.1016/j.ijrobp.2010.12.032
28. Song CW, Kim H, Cho H, et al. HIF-1 α Inhibition Improves Anti-Tumor Immunity and Promotes the Efficacy of Stereotactic Ablative Radiotherapy (SABR). *Cancers (Basel)*. 2022;14(13):3273. doi:10.3390/cancers14133273
29. Dewhirst MW, Cao Y, Moeller B. Cycling hypoxia and free radicals regulate angiogenesis and radiotherapy response. *Nat Rev Cancer*. 2008;8(6):425-437. doi:10.1038/nrc2397
30. Baud O, Haynes RF, Wang H, et al. Developmental up-regulation of MnSOD in rat oligodendrocytes confers protection against oxidative injury. *Eur J Neurosci*. 2004;20(1):29-40. doi:10.1111/j.0953-816X.2004.03451.x
31. Back SA, Gan X, Li Y, Rosenberg PA, Volpe JJ. Maturation-dependent vulnerability of oligodendrocytes to oxidative stress-induced death caused by glutathione depletion. *J Neurosci*. 1998;18(16):6241-6253. doi:10.1523/jneurosci.18-16-06241.1998
32. Yuen TJ, Silbereis JC, Griveau A, et al. Oligodendrocyte-encoded HIF function couples postnatal myelination and white matter angiogenesis. *Cell*. 2014;158(2):383-396.

doi:10.1016/j.cell.2014.04.052

33. Fuchs EJ, O'Donnell PV, Eapen M, et al. Double unrelated umbilical cord blood vs HLA-haploidentical bone marrow transplantation: the BMT CTN 1101 trial. *Blood*. 2021;137(3):420-428.
doi:10.1182/blood.2020007535
34. Koreth J, Schlenk R, Kopecky KJ, et al. Allogeneic stem cell transplantation for acute myeloid leukemia in first complete remission: systematic review and meta-analysis of prospective clinical trials. *Jama*. 2009;301(22):2349-61. doi:10.1001/jama.2009.813
35. Stanaszek L, Rogujski P, Drela K, et al. Transplantation of Human Glial Progenitors to Immunodeficient Neonatal Mice with Amyotrophic Lateral Sclerosis (SOD1/rag2). *Antioxidants (Basel)*. 2022;11(6):1050. doi:10.3390/antiox11061050
36. Baloh RH, Johnson JP, Avalos P, et al. Transplantation of human neural progenitor cells secreting GDNF into the spinal cord of patients with ALS: a phase 1/2a trial. *Nat Med*. 2022;28(9):1813-1822.
doi:10.1038/s41591-022-01956-3

Figures

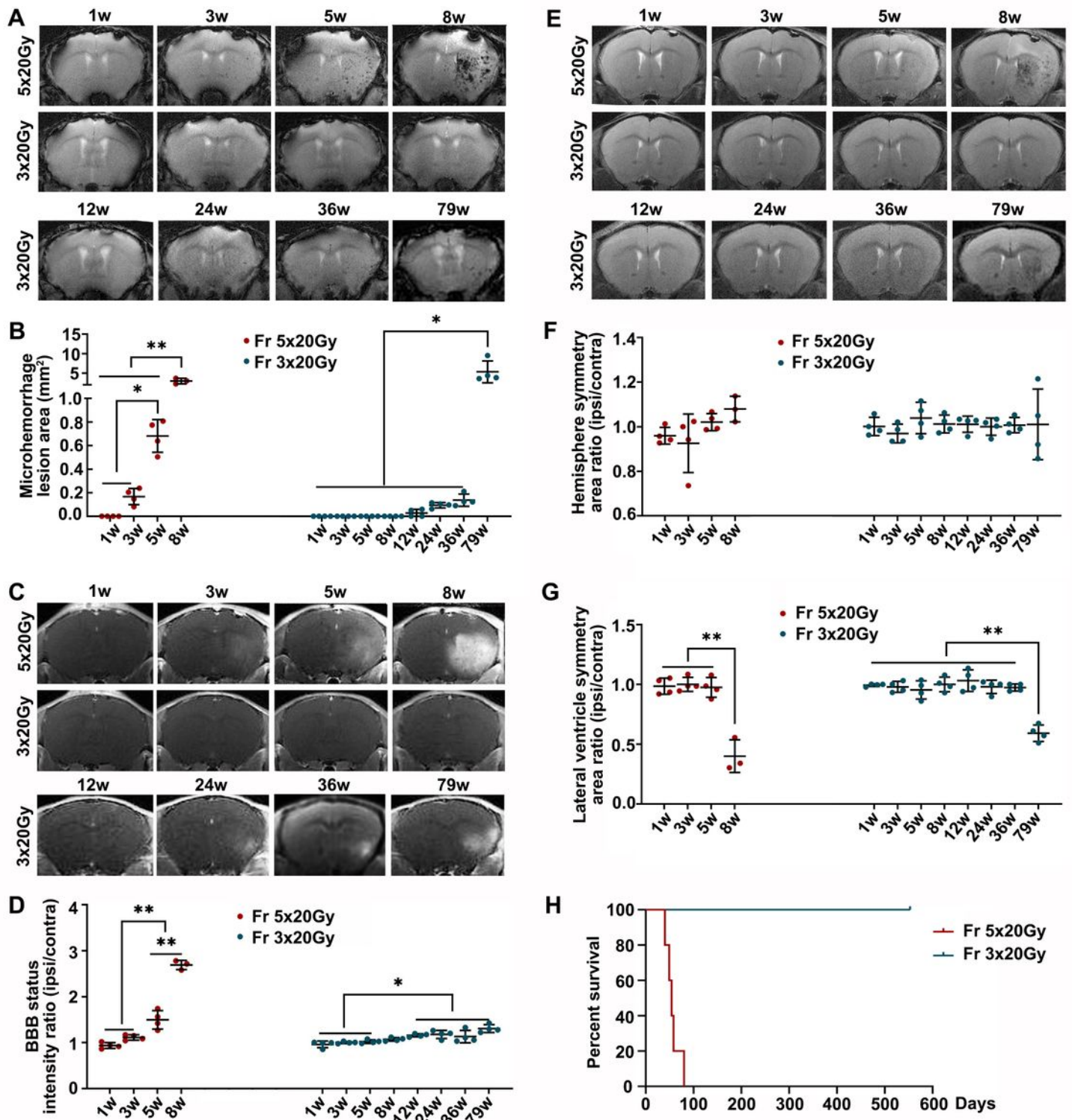


Figure 1

Monitoring radiation-induced brain injury after ultra-high fractionated 5x20 Gy and 3x20 Gy with longitudinal MRI. (A-B) Representative T2* images and microhemorrhage assessment for mice receiving fractionated radiation. (C-D) Representative T1-weighted gadolinium-enhanced MR images and BBB status for mice receiving fractionated radiation. (E-G) Representative T2-weighted MR images and

anatomical analysis for mice receiving fractionated radiation. ANOVA. N=4 mice/group. *P<0.05, **P<0.01. (H) Kaplan-Meier curves of mice receiving radiation. N=5 mice/group.

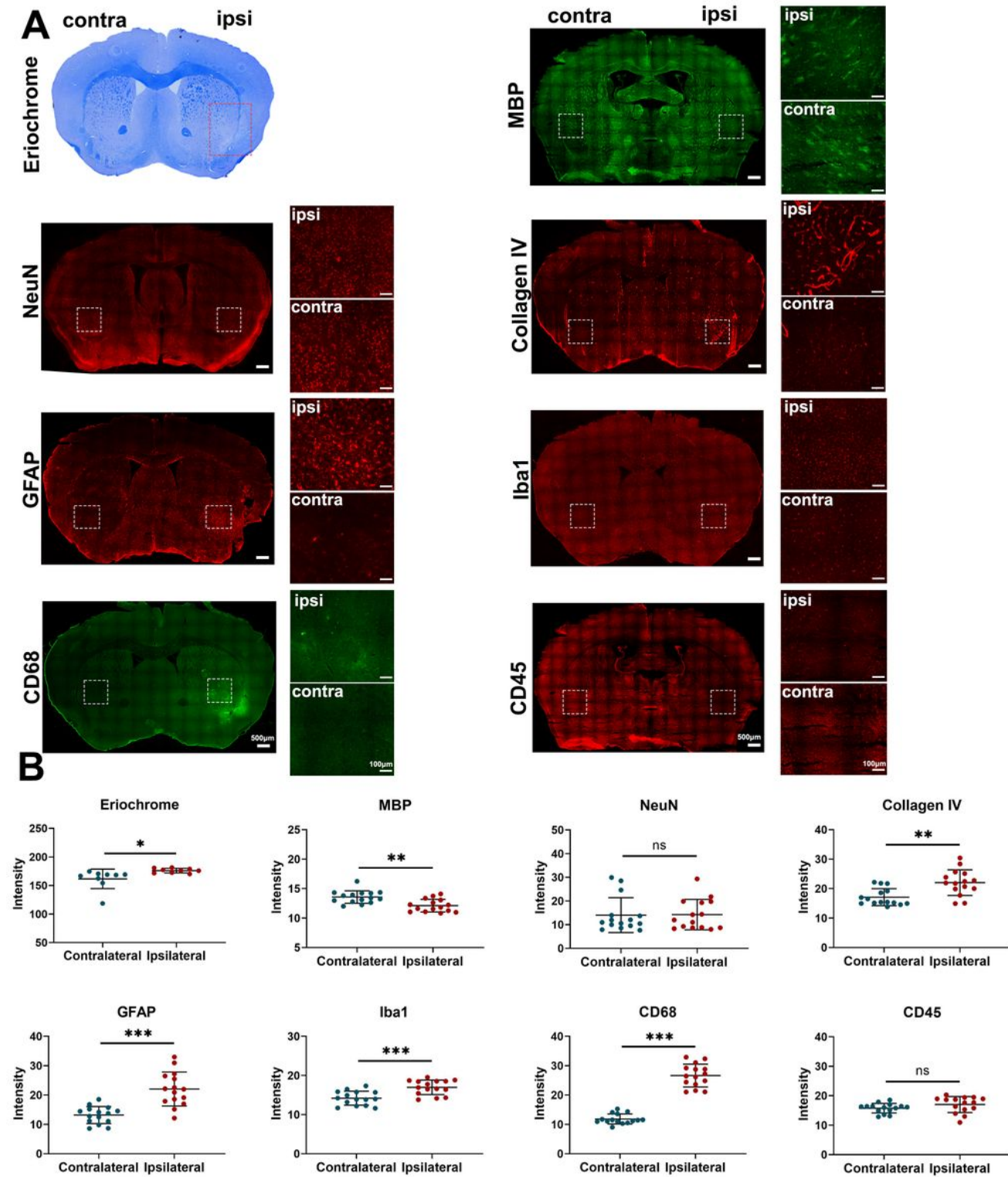


Figure 2

Histological evidence of brain damage after fractionated 3x20 Gy radiation. (A) Representative histology/immunohistochemistry of brain tissue stained for Eriochrome, MBP, NeuN, Collagen IV, GFAP,

Iba1, CD68, and CD45 at 80 weeks after fractionated 3×20 Gy radiation. The scale bars are 500 μm for low-power images and 100 μm for high-power images. (B) Quantification of signal intensity in the contralateral and ipsilateral hemispheres for each staining. Paired t-test. N=3 ROIs from 3 (ErioChrome staining) or 5 (all the immunofluorescence staining) brain slices in each group. *P<0.05, **P<0.01, ***P<0.001. ns: no significant difference.

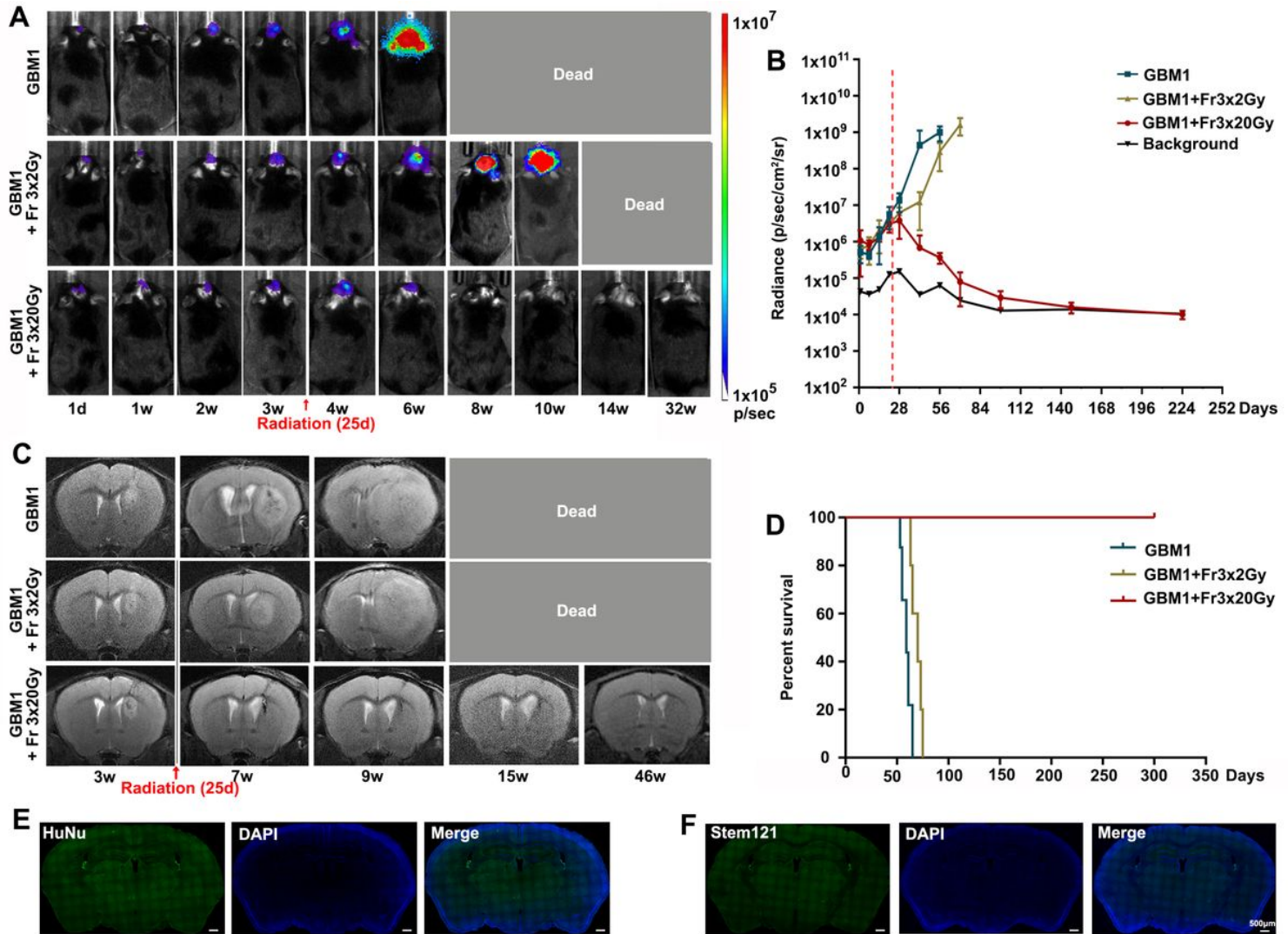


Figure 3

Eradiation of GBM1 tumor with high-dose radiotherapy. (A) Representative BLI images of non-irradiation, fractionated 3×2 Gy or 3×20 Gy irradiation-treated tumor-bearing mice at the indicated days. Irradiation was started on day 25 after tumor inoculation. (B) Quantification of the BLI signal revealed that 3×20 Gy radiation completely eradicates the GBM1 tumor. The dot-dashed line represents the date of starting radiation. (C) Representative T2-weighted MR images for GBM1 mice without radiation or with fractionated 3×2 Gy or 3×20 Gy radiation. (D) Survival curves of GBM1 mice with or without radiation. N=5 mice/group. (E) HuNu staining. (F) Stem 121 staining. The scale bars are 500 μm.

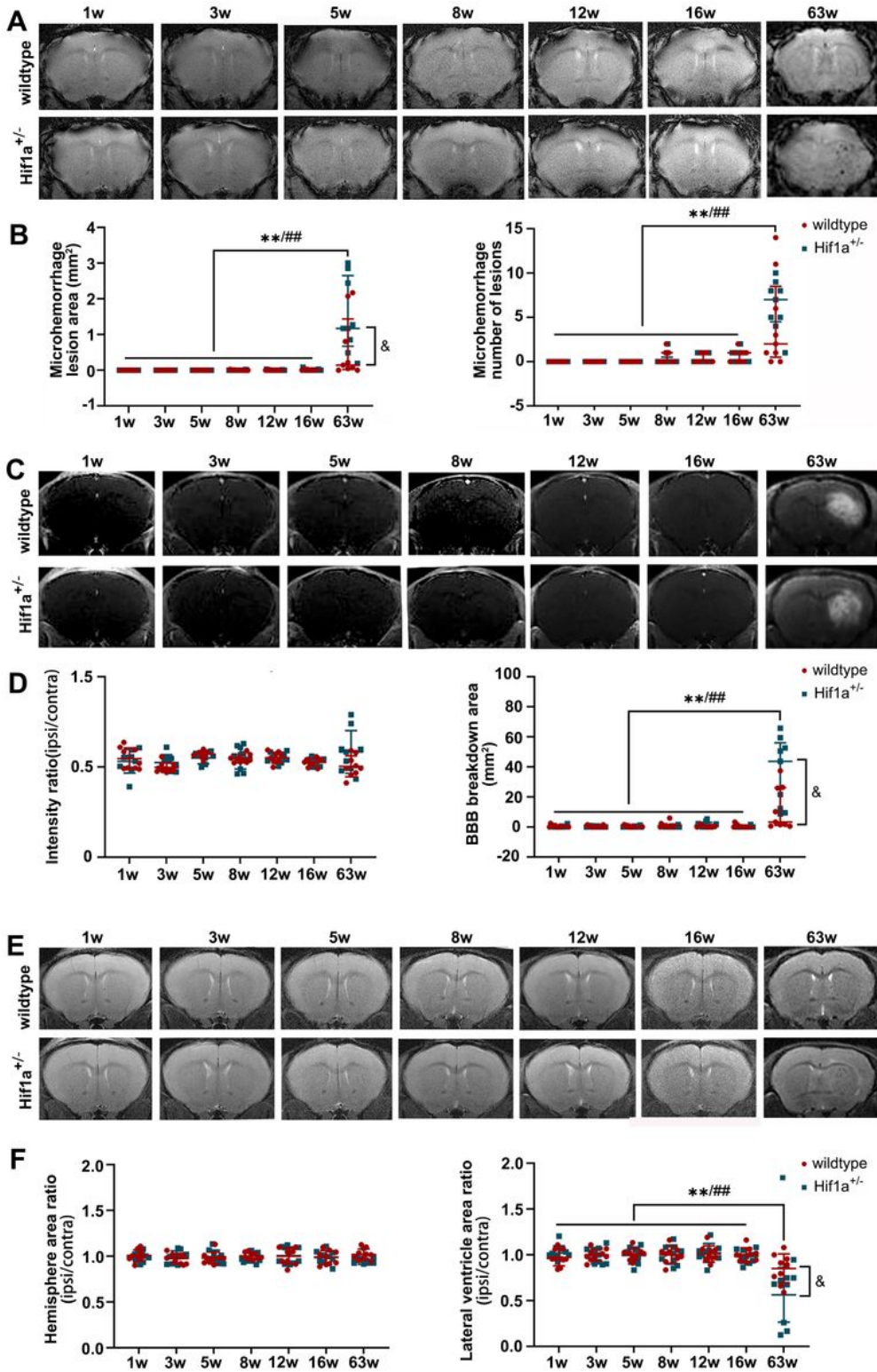


Figure 4

Under longitudinal MRI, monitoring brain damage after fractionated 3×20 Gy radiation in both HIF-1α^{+/-} heterozygote and wild-type mice. (A-B) Representative T2* images and microhemorrhage assessment for mice receiving fractionated radiation. (C-D) Representative T1-weighted gadolinium-enhanced MRI and BBB status for mice receiving fractionated radiation. (E-F) Representative T2-weighted MR images and anatomical analysis for mice receiving fractionated radiation. N=3 mice per group (3 slices for each

mouse). Wildtype group: $^{*/*}P$ 0.05/0.01. HIF-1 $\alpha^{+/-}$ group: $\#/\#\#P$ 0.05/0.01. wildtype vs. HIF-1 $\alpha^{+/-}$ group: $\&P$ 0.05.

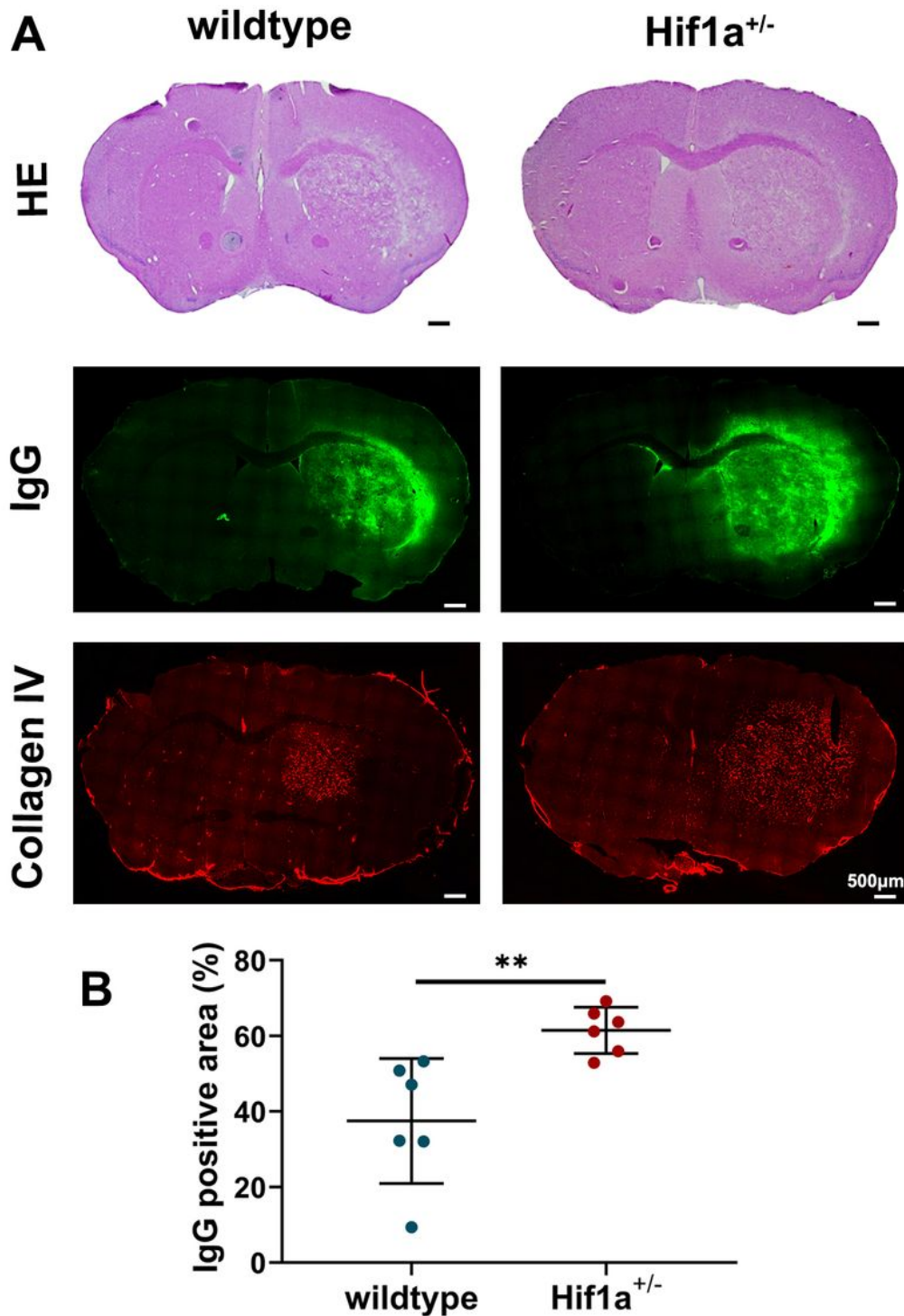


Figure 5

HIF-1 α gene deficiency exacerbates vascular damage after radiation. (A) Representative H&E staining, IgG, and Collagen IV immunostaining for wild-type and HIF-1 $\alpha^{+/-}$ mice. The scale bars are 500 μ m. (B)

Quantification of the percentage of IgG positive staining area in ipsilateral hemisphere area. Student t-test. N=6 brain slices in each group. **P<0.01.

Supplementary Files

This is a list of supplementary files associated with this preprint. Click to download.

- [SupplementaryFigure1.jpg](#)
- [SupplementaryFigure2.jpg](#)